frontiers | Frontiers in Plant Science

TYPE Original Research
PUBLISHED 11 December 2024
DOI 10.3389/fpls.2024.1504404

OPEN ACCESS

EDITED BY
Didier Reinhardt,
University of Fribourg, Switzerland

REVIEWED BY
Rene Geurts,
Wageningen University and Research, Netherlands
Jesus Montiel,
National Autonomous University of Mexico, Mexico
Jeremy Dale Murray,
Shanghai Institutes for Biological Sciences (CAS), China

*CORRESPONDENCE
Julia A. Frugoli
jfrugol@clemson.edu

†PRESENT ADDRESSES
Diptee Chaulagain,
Department of Bioengineering, Clemson University, Clemson, SC, United States
Elise Schnabel,
Department of Plant and Environmental Sciences, Clemson University, Clemson, SC, United States

RECEIVED 30 September 2024
ACCEPTED 11 November 2024
PUBLISHED 11 December 2024

CITATION
Chaulagain D, Schnabel E, Kappes M, Lin EX, Müller LM and Frugoli JA (2024) *TML1* and *TML2* synergistically regulate nodulation and affect arbuscular mycorrhiza in *Medicago truncatula*.
Front. Plant Sci. 15:1504404.
doi: 10.3389/fpls.2024.1504404

TML1 and *TML2* synergistically regulate nodulation and affect arbuscular mycorrhiza in *Medicago truncatula*

Diptee Chaulagain[1†], Elise Schnabel[1†], Mikayla Kappes[2], Erica Xinlei Lin[3], Lena Maria Müller[2,3] and Julia A. Frugoli[1*]

[1]Department of Genetics and Biochemistry, Clemson University, Clemson, SC, United States, [2]Plant Molecular and Cellular Biology Laboratory, Salk Institute for Biological Studies, La Jolla, CA, United States, [3]Department of Biology, University of Miami, Coral Gables, FL, United States

Two symbiotic processes, nodulation and arbuscular mycorrhiza, are primarily controlled by the plant's need for nitrogen (N) and phosphorus (P), respectively. Autoregulation of nodulation (AON) and autoregulation of mycorrhizal symbiosis (AOM) both negatively regulate their respective processes and share multiple components—plants that make too many nodules usually have higher arbuscular mycorrhiza (AM) fungal root colonization. The protein TML (TOO MUCH LOVE) was shown to function in roots to maintain susceptibly to rhizobial infection under low N conditions and control nodule number through AON in *Lotus japonicus*. *Medicago truncatula* has two sequence homologs: *Mt*TML1 and *Mt*TML2. We report the generation of stable single and double mutants harboring multiple allelic variations in *MtTML1* and *MtTML2* using CRISPR–Cas9 targeted mutagenesis and screening of a transposon mutagenesis library. Plants containing single mutations in *Mt*TML1 or *Mt*TML2 produced two to three times the nodules of wild-type plants, whereas plants containing mutations in both genes displayed a synergistic effect, forming 20× more nodules compared to wild-type plants. Examination of expression and heterozygote effects suggests that genetic compensation may play a role in the observed synergy. Plants with mutations in both *TML*s only showed mild increases in AM fungal root colonization at later timepoints in our experiments, suggesting that these genes may also play a minor role in AM symbiosis regulation. The mutants created will be useful tools to dissect the mechanism of synergistic action of *Mt*TML1 and *Mt*TML2 in *M. truncatula* symbiosis with beneficial microbes.

KEYWORDS

nodulation, mycorrhization, *Medicago truncatula*, AON, AOM, TML

Introduction

Since plants are sessile and require nutrients from the soil, they have developed strategies to maximize survival when the supply of nutrients is variable (Oldroyd and Leyser, 2020). Legume plants can grow in nitrogen (N)-poor soil using an additional strategy beyond those of most dicots: legumes can establish an endosymbiosis with rhizobial bacteria, which allows the N fixed from the atmosphere by the bacteria to be shared with the plant. Rhizobia are harbored in specialized root organs called nodules. The establishment of the legume root nodule symbiosis is tightly regulated, including by species-specific signals from the rhizobia (lipo-chitooligosaccharides) and internal plant signaling related to the carbon and N status of the plant. Obtaining N through symbiosis is energetically costly to the plant, resulting in regulation based on both available soil N, which appears to use common signals among most plants (Oldroyd and Leyser, 2020), and already established nodulation, which uses a pathway called autoregulation of nodulation (AON) to control the number of nodules that form on a legume (reviewed in Ferguson et al., 2019; Roy et al., 2020; Chaulagain and Frugoli, 2021).

The AON pathway negatively controls nodule number through systemic signal transduction and has been studied in many species; here, we used *Medicago truncatula* nomenclature. Upon inoculation of *M. truncatula* with rhizobia, genes encoding the signaling peptides MtCLE12 and MtCLE13 are induced in the root (Mortier et al., 2010) through activation by NIN (Laffont et al., 2020). All CLE peptides undergo proteolytic processing from the original gene transcripts (see Gao and Guo, 2012, and Roy and Müller, 2022, for review), and MtCLE12 is additionally post-translationally glycosylated by the MtRDN1 enzyme before being translocated to the shoot (Kassaw et al., 2017). In the shoot, these CLE peptides are ligands for the leucine-rich receptor-like kinase (LRR-RLK) *M. truncatula* SUNN (SUPERNUMERARY NODULES) (Mortier et al., 2012). SUNN, which is the *M. truncatula* ortholog of *Arabidopsis* CLAVATA1, forms a putative complex with the pseudo kinase CORYNE (CRN) and the receptor protein CLAVATA2 (CLV2) (Crook et al., 2016). MtCLE12,13/SUNN signaling results in increased transport of cytokinin and decreased expression the of shoot-to-root signal miR2111 (Tsikou et al., 2018; Okuma et al., 2020; Okuma and Kawaguchi, 2021).

Based on the mutational analysis in *Lotus japonicus*, which has only one *TML* (*TOO MUCH LOVE*) gene and RNA interference (RNAi) in *M. truncatula*, which has two, reduced levels of miR2111 in roots correspond with the increased expression of the *TML* genes, which encode F-box proteins that negatively regulate nodule number (Magori et al., 2009; Tsikou et al., 2018; Gautrat et al., 2019). The downregulation effect of miR2111 on *TML* transcripts is postulated based on several lines of evidence: 1) the presence of predicted binding sites for miR2111 in the 5′ end of the *TML* gene (Gautrat et al., 2020), 2) the observation that a miR2111 target mimic increases the *TML* transcript levels in a *sunn* mutant (Gautrat et al., 2020), and 3) increasing miR2111 levels through overexpression in roots increases nodule number and decreases the transcript levels of *TML* at 5 days post-inoculation (dpi) (Gautrat et al., 2021).

Like nodulation, plant interactions with arbuscular mycorrhiza (AM) fungi are also controlled by autoregulation and plant nutrient status. AM symbiosis occurs in most land plants, including 85%–90% of angiosperms; unlike nodulation, AM symbiosis is not restricted to legumes (Genre et al., 2020). The autoregulation and nutrient-regulated signaling pathways fine-tuning AM symbiosis share several, but not all, components and mechanisms with AON and N regulation of nodulation (Bashyal et al., 2024). In *M. truncatula*, autoregulation of mycorrhizal symbiosis (AOM) is mediated by the AM-induced peptide MtCLE53, which elicits a negative feedback loop that represses AM symbiosis in concert with the LRR-RLK SUNN (Müller et al., 2019; Karlo et al., 2020). Components of AOM are conserved beyond the legume clade: hyper-mycorrhizal mutants—characterized by elevated overall root length colonization and arbuscule numbers—in CLE peptides and orthologs of SUNN and CLV2 have been described not only in the legumes *M. truncatula*, soybean, pea, and *L. japonicus* but also in the non-legumes *Brachypodium distachyon* and tomato (Morandi et al., 2000; Zakaria Solaiman et al., 2000; Meixner et al., 2005; Wang et al., 2018; Müller et al., 2019; Karlo et al., 2020; Wang et al., 2021). Notably, recent research revealed the existence of multiple parallel CLAVATA signaling pathways modulating AM symbiosis (Orosz et al., 2024; Wulf et al., 2024).

AM symbiosis is also regulated by plant P and N status. Accumulating evidence suggests that P- and N-induced CLE peptides contribute to nutrient regulation of AM symbiosis; although our knowledge is still fragmented, at least some of the nutrient-regulated CLE peptides require the same LRR-RLKs or other regulators of AOM and AON (Müller et al., 2019; Wang et al., 2021).

Thus far, *TML* is the only gene with a loss of function hypernodulation mutant phenotype reported to function downstream of the SUNN LRR-RLK in the AON pathway and was first described in *L. japonicus* (Magori et al., 2009). No mutation of a gene downstream of SUNN resulting in a hyper-mycorrhizal phenotype has been reported in AOM. The *L. japonicus tml* mutant plants form ~8× more nodules spreading across larger areas of root than the wild type, a phenotype governed by root genotype (Magori et al., 2009). The gene encodes a protein containing a Nuclear Localization Signal (NLS), F-box domain, and kelch repeats (Takahara et al., 2013). Previous work demonstrated that overexpression of *MtCLE12* and *MtCLE13* results in the induction of *MtTML1* and *MtTML2* expression even in the absence of rhizobia (Gautrat et al., 2019). In addition, MtCEP1 (*C-TERMINALLY ENCODED PEPTIDE1*) generated in response to low N requires the MtCRA2 (*COMPACT ROOT ARCHITECTURE2*) receptor to upregulate miR2111 expression in the shoots and hence lower the transcript level of both *MtTML*s to maintain root competence to nodulation (Gautrat et al., 2020).

The presence of kelch repeats and F-box domains in TML proteins suggest that TMLs could bind to each other, as well as target other proteins for proteasomal degradation; however, biochemical studies to identify such targets have not occurred yet. Genetic studies in *M. truncatula* have been hindered by the lack of stable mutants and have been limited to RNAi experiments and measuring transcript levels (Gautrat et al., 2019, 2020). To understand the role of two TML proteins in nodulation, mutant analysis is critical. We obtained a mutant in *MtTML2*, *tml2-1*, from a *Tnt1* transposon insertion mutant library (Tadege et al., 2008) and

generated stable single and double mutants harboring multiple allelic variations in *MtTML1* and *MtTML2* using CRISPR–Cas9 targeted mutagenesis. Plants containing mutations in a single *MtTML* gene displayed two to three times as many nodules as wild-type plants; however, plants containing mutations in both genes displayed a synergistic effect, with up to 20-fold more nodules than the wild-type plants. By contrast, AM fungal root colonization was only mildly enhanced in a *tml* double mutant; furthermore, this effect was dependent on the timepoint measured and the mutant allele. Taken together with observations on gene expression and other phenotypes reported below, our findings demonstrate the requirement of both *MtTML1* and *MtTML2* in controlling nodule number through synergistic signaling in nodulation with an additional minor role in AM symbiosis regulation under the experimental conditions tested.

Materials and methods

Plant growth conditions

Seeds were germinated as described previously (Schnabel et al., 2010). Briefly, seeds were scarified using concentrated sulfuric acid, imbibed in water, vernalized at 4°C for 2 days, and allowed to germinate overnight at room temperature in the dark. One-day-old seedlings were placed in an aeroponic chamber and grown at 21°C–25°C on a 14-hour/10-hour light/dark cycle and inoculated as described in Cai et al. (2023). To determine nodulation phenotypes, no N was included in the media, and plants were inoculated with *Sinorhizobium meliloti* RM41 (Putnoky et al., 1990) 4 days post-germination as indicated. Nodule count and root length measurements were performed at 10 dpi. For seed collection and genetic crosses, plants were grown in a greenhouse with supplemental light on a 14-hour/10-hour light/dark cycle at 21°C–25°C. For mycorrhizal assays, seed germination and inoculation with *Rhizophagus irregularis* were performed as previously described (Chaulagain et al., 2023). In brief, 3-day-old seedlings were planted in Cone-tainers SC10R (Stuewe and Sons, Tangent, OR, USA) and placed in a growth chamber on a 16-hour/8-hour light/dark cycle at 22°C–24°C and 40% humidity. The growth mixture was 50% play sand (Quikrete, Atlanta, GA, USA) and 50% fine vermiculite (Ferry-Morse, Norton, MA, USA). All substrate components were washed in distilled water and autoclaved for 55 min before use. For colonization with *R. irregularis*, 250 spores (Premier Tech, Rivière-du-Loup, QC, Canada) were placed 5 cm below the surface in a layer of fine sand. All plants were treated twice a week with 15 mL of half-strength, low Pi Hoagland's fertilizer (20 µM phosphate) to aid in symbiosis initiation. Plants were harvested 4.5 or 6 weeks post-planting.

Tnt1 mutant screening and verification of insert

Tnt1 insertion lines created by *Tnt1* mutagenesis of the R108 ecotype (Tadege et al., 2008) were screened electronically for insertions in *MtTML* genes. While no *MtTML1* insertion lines were identified, a pool of plants contained a mutation in the *MtTML2* gene in *M. truncatula* (NF0679; Noble Foundation Medicago Mutant Database, now located at https://medicagomutant.dasnr.okstate.edu/mutant/index.php). Seeds from the NF0679 pool were grown in the greenhouse, and a line containing the insertion in the second exon was identified by PCR using primers from Supplementary Table 2. The line was selfed to yield homozygotes, which were then backcrossed to the R108 wild type and re-isolated. The amplicons generated by primers 2189/1925 and 2690/3227 were sequenced to determine the exact position of the *Tnt1* insertion in relation to the gene. This line is called *tml2-1*.

Constructs for CRISPR–Cas9 mutagenesis

Multi-target constructs were designed for *MtTML1* alone and to target both *MtTML* genes in the same plant (Supplementary Figure 1). Two target sites per gene were chosen following the target selection criteria (Ma and Liu, 2016). Sites unique to the *MtTML* genes were selected to avoid off-target mutagenesis by comparison to the *M. truncatula* genome MtV4.0 (Tang et al., 2014). The binary vector pDIRECT_23C (Čermák et al., 2017) (Addgene) was used as a Cas9-containing vector. The target and gRNA were cloned into the pDIRECT_23C vector, and the finished construct was created using Golden Gate assembly (Engler et al., 2008, 2009) following the protocol in Čermák et al. (2017). The resulting vectors pDIRECT_23C+MtTML1 (containing two targets for *MtTML1*) and pDIRECT_23C+MtTML1/2 (containing two targets each for *MtTML1* and *MtTML2*) were then verified by sequencing. A verified clone in *Escherichia coli* (Zymo 10B, Zymo Research, Irvine, CA, USA) was used as a plasmid source to move each construct into *Agrobacterium tumefaciens* EHA105 (Hood et al., 1993) for use in plant transformation.

Generation of transgenic plants using CRISPR–Cas9 mutagenesis

To obtain alleles of *MtTML1*, additional alleles of *MtTML2*, and plants containing mutations in both genes, CRISPR–Cas9 mutagenesis of embryonic callus tissue followed by regeneration of whole plants was performed in the R108 ecotype. Each construct was introduced with *Agrobacterium*-mediated transformation into root segments of 4–7-day-old R108 seedlings and taken through callus and tissue culture following the protocol 2A of Wen et al. (2019) with the following modifications for selection and rooting: the selection of phosphinothricin (ppt)-resistant callus used 2 mg/L ppt in the media, and 2 mg/L NAA was used in RCTM6 medium described in Wen et al. (2019) for rooting. All plants originating from a callus were considered one independent line. The three most developed plants at the rooting medium stage for each line per callus were transferred into the soil for acclimatization and grown to collect seeds.

Transgenic verification, genotyping, and segregation of targeted mutagenesis in T1 generation

All T0 lines generated from tissue culture were screened by PCR for the presence of the transgene using Cas9-specific primers (primers 3081/3082; Supplementary Table 2), and lines testing positive were then screened by PCR for deletions using gene-specific primers (Supplementary Table 2). The deletion was confirmed by the size difference of an amplicon after gel electrophoresis. All the amplicons were sequenced using the same primers as for the PCR to determine the exact mutations.

All T0 lines containing mutations were allowed to set seeds. The T1 generation was screened for plants homozygous for a single allele by PCR. All amplicons were sequenced to confirm homozygosity and sequence. To generate the *tml1 tml2* double mutant transgenic lines, a T0 line carrying two mutant alleles for each gene was used. All alleles except *tml1-4* were backcrossed once to R018, and all alleles including the homozygous double mutants did not have detectable Cas9 when tested by PCR amplification.

Real-time PCR analysis of MtTML in mutant plants

RNA was extracted from 10 roots of each of the mutants and R108 [wild type (WT)] was harvested at 10 days post-inoculation with RM41. Root tissue was frozen at −80°C until RNA extraction. Root tissue from six plants pooled together for each genotype was ground in liquid nitrogen and 100 mg of tissue was used for RNA extraction. RNA was extracted using TRIzol® Reagent (Life Technologies, Carlsbad, CA, USA) followed by DNase digestion using RQ1 RNase-free DNase (Promega, Madison, WI, USA) according to the manufacturer's instructions. cDNA was synthesized using iScript™ Reverse Transcriptase (Bio-Rad, Hercules, CA, USA) according to the manufacturer's instructions. Real-time qPCR was performed in 10-µL reactions in an iQ5 instrument (Bio-Rad, CA, USA) using iTaq™ Universal SYBR® Green Supermix (Bio-Rad, CA, USA) and a 400-nM final concentration of each primer (Supplementary Table 2) Each reaction was run in three technical and three biological replicates. Relative expression levels of genes were assayed using the Pfaffl method (Pfaffl 2001) relative to a previously validated housekeeping reference gene phosphatidylinositol 3- and 4-kinase belonging to the ubiquitin family (PI4K; Medtr3g091400 in MtV4.0, MtrunA17Chr3g0126781 in MtrunA17r5.0-ANR) (Kakar et al., 2008). Data from the three biological replicates were used to estimate the mean and standard error.

DNA isolation

DNA was isolated from leaf presses made by pressing a leaflet of each plant to a Plant Card (Whatman™, GE Healthcare UK Limited, Amersham, UK) for long-term storage. A 1.2-mm-diameter piece of Plant Card was excised and washed with Whatman™ FTA Purification Reagent (GE Healthcare UK Limited, UK) followed by TE-1 buffer according to the manufacturer's instructions and directly used in PCR. DNA from the R108 wild type used multiple times was isolated using the DNeasy Plant Mini Kit (Qiagen, Hilden, Germany) as per the manufacturer's instruction.

PCR conditions

All amplifications except for use in cloning were performed using GoTaq® G2 DNA Polymerase (Promega Corporation, Madison, USA) following the manufacturer's instructions and buffers. Standard PCR conditions used were as follows: 2 min at 95°C, 35 cycles (10 s at 95°C, 15 s at gene-specific annealing temperature, 30 s/Kb at 72°C), 5 min at 95°C. When using a leaf press as a DNA template for amplification, cycles were increased from 35 to 40. The gene-specific annealing temperature was 55°C except as noted for primer pairs 3148/3149 (58°C), 3182/3183 (52°C), and 2493/2494 (56°C). Annealing temperatures were predicted using the "Tm Calculator" tool available at https://www.thermofisher.com/. Amplification of inserts for cloning was performed using iProof™ High-Fidelity DNA Polymerase (Bio-Rad Laboratories, USA) and buffers according to the manufacturer's instructions.

Imaging

Nodule images were taken using the Leica Microsystems THUNDER Imager Model Organism with the attached DMC4500 color camera. For visualization of AM fungal structures, colonized roots were cleared in 20% KOH (w/v) at 65°C for 2 days. Then, they were rinsed three times with ddH_2O for at least 1 day until the roots appeared white, and the pH was neutralized overnight using 1× phosphate-buffered saline (PBS). Cleared roots were stained in Alexa Fluor® 488 wheat germ agglutinin (WGA)–PBS solution, so the final concentration of WGA was 0.2 µg/mL. AM fungal root colonization was quantified using the grid-line intersections method using a stereomicroscope and a gridded square petri dish (Sparling and Tinker, 1978; Giovannetti and Mosse, 1980). Images were captured using a Leica M205 stereoscope.

Computational and statistical analyses

The phylogenetic in tree was generated with (MEGA11) (Tamura et al., 2021) using the maximum likelihood method and tested using bootstrap for 1,000 replicates. The normality of data was tested by fitting a normal curve before performing the statistical tests. Tukey's comparison for all pairs was used for comparison among more than two groups, and Student's t-test was used for comparing two groups for normal data. The non-parametric Steel–Dwass comparison for all pairs was used for the analysis of non-normal data. Statistical test was performed using JMP Pro 17.1.

10.3389/fpls.2024.1504404

Results

The number of TML genes in a genome is not correlated with the ability to nodulate or the nodule meristem type

Since only one *TML* gene has been identified in *L. japonicus* (Magori et al., 2009), which forms determinate nodules, we wondered if having two copies of *TML*, like *M. truncatula* (Gautrat et al., 2019), was correlated with indeterminate nodulation and whether multiple copies appear in non-nodulating plants. Figure 1 displays a maximum likelihood tree for amino acid sequence homologs of LjTML identified by BLASTP in selected determinate and indeterminate nodule-forming legumes, non-legume dicots, and monocots. TML proteins from legumes clustered in a separate branch from non-legumes, while single TMLs from the monocots rice, maize, and sorghum clustered separately forming the tree root; these species have only ~40% amino acid sequence similarity with LjTML. In cases where non-legumes had two TML proteins, with similar low similarity scores to both TML1 and TML2, the labels are based on previous descriptions or ploidy. *Arabidopsis* does not form either symbiotic association with rhizobia or mycorrhizae, and the *Arabidopsis* protein *At*HOLT (*HOMOLOG OF LEGUME TML*) has only 51% amino acid sequence identity to LjTML, yet the *AtHOLT* transcript is a target of miR2111 (Hsieh et al., 2009; Pant et al., 2009) and regulates lateral root formation in response to nitrate in the same manner as *Lj*TML. There is no correlation among legumes between *TML* gene number and nodule meristem type. Only one gene encoding a TML protein was identified by BLAST search in the determinate nodulating species *L. japonicus* and *Phaseolus vulgaris* (common bean), whereas determinate nodulating soybean has genes encoding three TML proteins. *GmTML1a* and *GmTML1b* are gene duplicates sharing 93.32% sequence identity, and the encoded proteins cluster together in the phylogenetic tree, likely the result of the partially diploidized tetraploid soybean genome (Shultz et al., 2006). The same a, b designation used for the soybean duplicate proteins was applied to *Nicotiana tabacum*, a recent allotetraploid of *Nicotiana sylvestris* and *Nicotiana tomentosiformis* (Renny-Byfield et al., 2011) and *Populus trichocarpa*, which underwent a whole genome duplication approximately 60 million years ago (Dai et al., 2014). The TML2 protein sequences in legumes (*Gm*TML2, *Mt*TML2, *Ps*TML2, and *Tp*TML2) cluster together and branch separately from TML1 sequences, suggesting that the two genes encoding TML proteins evolved from a common ancestral duplication in legumes, compared to the independent duplications in other dicots that form clades by species.

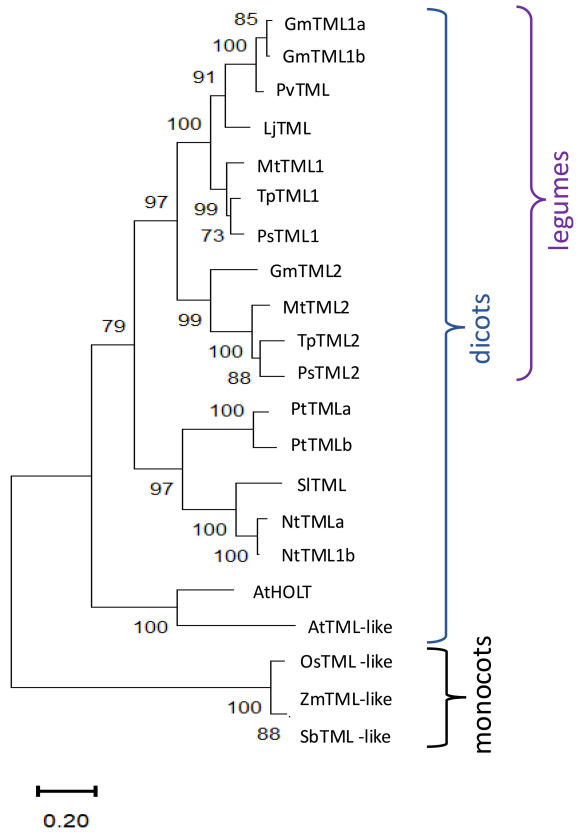

FIGURE 1
Phylogenetic analysis and structure of TML sequence homologs. Analysis by the maximum likelihood method using sequence homologs from public databases (Gene IDs in Supplementary Table 1) as described in Materials and Methods of in *Medicago truncatula* (Mt), *Arabidopsis thaliana* (At), *Nicotiana tabacum* (Nt), *Pisum sativum* (Ps), *Trifolium pratense* (Tp), *Glycine max* (Gm), *Phaseolus vulgaris* (Pv), *Solanum lycopersicum* (Sl), *Populus trichocarpa* (Pt), *Zea mays* (Zm), *Oryza sativa* (Os), and *Sorghum bicolor* (Sb). Percentage of replicate trees in which the associated taxa clustered together in the bootstrap test 1,000 replicates are shown next to the branches.

Identification of lines with mutations in MtTML genes

To explore the function of the two TML proteins in *M. truncatula*, mutant lines were created and isolated. The *tml2-1* allele was identified in the NF0679 pool from the *Tnt1* insertional mutagenesis library and isolated as a homozygous line (see Materials and Methods). Additional mutant alleles of *MtTML1* and *MtTML2*, as well as plants containing mutations in both genes, were generated by CRISPR–Cas9 mutagenesis of embryonic callus tissue followed by regeneration of whole plants in the R108 ecotype (see Materials and Methods). Multiple combinations of heterozygous and biallelic mutations were identified, and two individual alleles of each gene, as well as two double mutant combinations, were used in this study (Figure 2; Supplementary Figure 1). The *tml1* mutants created by CRISPR include a deletion in *tml1-1* resulting in a premature stop codon, which was recovered in the creation of a double mutant and only characterized in the *tml1-1 tml2-2* double mutant. The two other alleles of *tml1* were isolated and characterized as single mutants: *tml1-2*, which removes 111 aa from the N terminus of the protein, and *tml1-4*, a deletion eliminating the start codon. The *tml2* single mutants include a CRISPR-generated deletion and the above-described *Tnt1* insertion, both resulting in stops early in the protein. As a result, the *tml1-1*

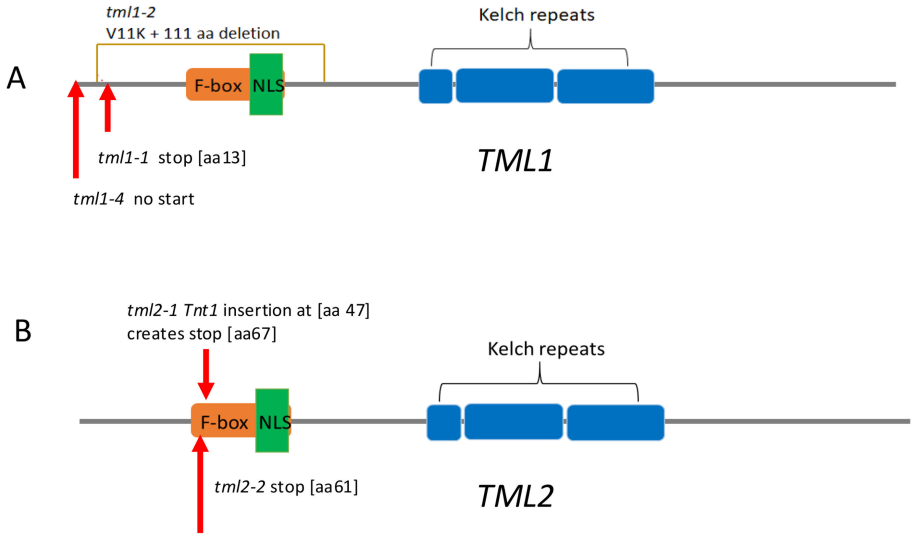

FIGURE 2
TML alleles used in this work. Diagrams are based on the translation of the R108 genotype sequence of Medtr7g029290 (*MtTML1*) and Medtr6g023805 (*MtTML2*). Protein features are shown by colored boxes: F-box in orange, kelch repeats in blue, and Nuclear Localization signal (NLS) in green. MiRNA2111 binding sites are in the coding sequence (CDS) indicated in Supplementary Figure 1. **(A)** *TML1* alleles. *tml1-2* is a 334-bp deletion with the addition of an A that results in a V-to-K change at amino acid 11, and deletion of 111 amino acids, removing the F-box and NLS. *tml1-4* is a 104-bp deletion in the 5′ UTR and beginning of the coding sequence that removes the start codon and the first 20 amino acids. **(B)** *tml2-1* is a *Tnt1* insertion 119 bp from the start of the coding region, resulting in addition of 20 new amino acids starting at position 47 before eventually terminating the protein at position 67. *tml2-2* is an insertion of a C, creating a stop codon at amino acid position 60 in the F-box.

tml2-2 double mutant is the combination of two early stops, and the *tml1-2 tml2-2* double mutant is the combination of an early deletion and a stop. All stops occur prior to or early in the F-box coding region, so that any resulting truncated protein is not expected to contain the F-box, NLS, and kelch repeats (Figure 2). The binding sites for miR2111 in *MtTML1* and *MtTML2* start at 143 bp and 134 bp into the CDS, respectively, and the binding site is lost only in the *tml1-4* mutant (Supplementary Figure 1).

MtTML1 and *MtTML2* single mutants have slightly increased nodule numbers while double mutants hypernodulate

The nodule number phenotypes of plants carrying mutant *tml1*, *tml2*, and *tml1 tml2* double mutant alleles were determined at 10 dpi with *S. meliloti* RM41 in an aeroponic system and compared to wild-type R108 plants and hypernodulating *sunn-5* plants (described in Crook et al., 2016; Nowak et al., 2019). Plants carrying a mutation in a single *MtTML* gene had more nodules than wild-type plants, while plants with mutations in both *MtTML* genes had many more nodules and shorter roots than wild-type plants (Figure 3A). All single mutant lines formed pink nodules similar in size to wild-type plants (Figures 3B–F), whereas the double mutant plants formed small, fused nodules in a wider area of the root (Figures 3G, H). Most nodules in the double mutants were white at 10 dpi, except for a few slightly pink nodules, indicating leghemoglobin production. No obvious shoot phenotype was observed in any line.

All mutants in a single *MtTML* gene formed a significantly higher number of nodules than the wild type but less than the known hypernodulating *sunn-5* mutant ($p \leq 0.01$, Steel–Dwass method of pairwise comparison; Figure 4A). The evaluation of nodules per cm of root length followed the same pattern as the total number of nodules (Figure 4B). However, the double mutants formed a significantly higher number of total nodules and nodules per cm of root length than both the wild type and *sunn-5* mutant (Figures 4C, D). The single mutants on average formed twofold to threefold more nodules, while the double mutants formed greater than 20-fold more nodules compared to the wild type (Figure 4).

MtTMLs differ in their spatiotemporal expression during nodule development

Using the ePlant resource for early nodulation (Schnabel et al., 2023) and past transcriptomics work in our lab (Schnabel et al., 2023), we examined the expression of the two *MtTML* genes in root segments during the first 72 hours responding to rhizobia (Figure 5). The genes were expressed in wild-type plants at low levels at the 0-hour timepoint, which were 4-day-old N-starved plants in our experimental system, but the expression increased in the vascular tissue for both genes at 12 hpi and 24 hpi (Figure 5A). By 48 hpi, when the nodules began to form, *MtTML1* was expressed at a similar level in the vascular, cortical, and epidermal laser-captured cells as well as the developing nodule cells, while *MtTML2* increased to a higher level in the vascular and inner cortical cells at

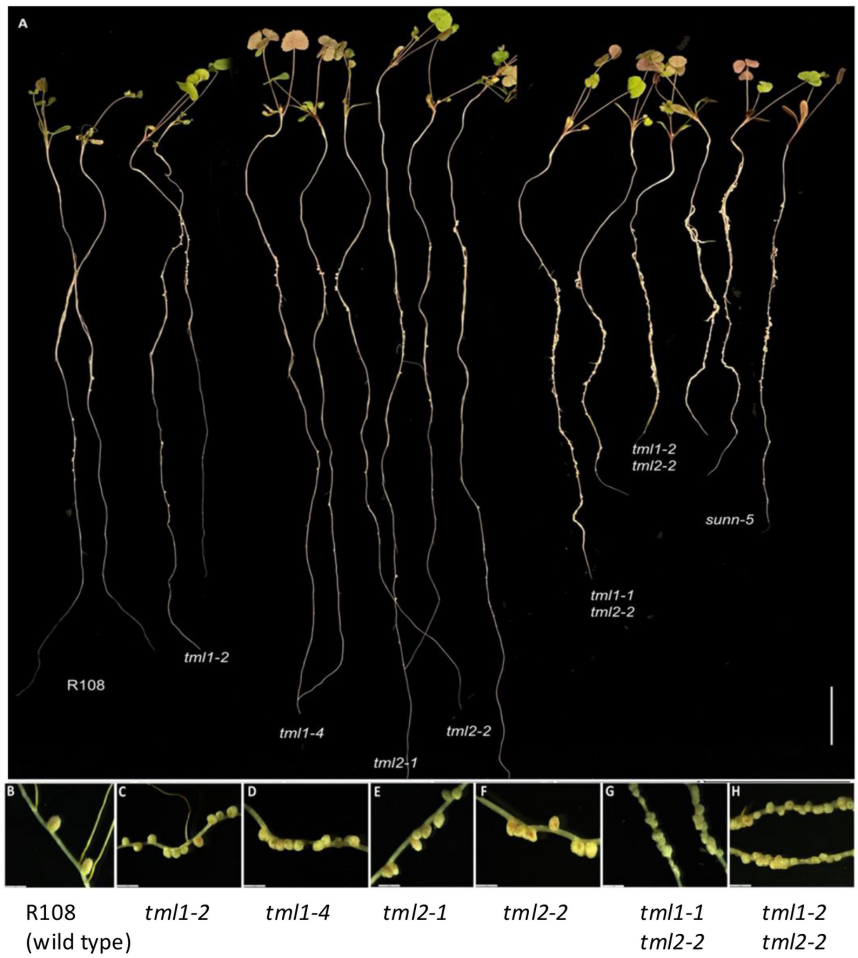

FIGURE 3
Phenotype of single and double mutant alleles in *MtTML1* and *MtTML2* genes. **(A)** Whole plants displaying root nodules at 10 dpi in an aeroponic system inoculated with *Sinorhizobium meliloti* strain RM41. Two representative plants per genotype L to R: R108 (wild type), *tml1-2*, *tml1-4*, *tml2-1*, *tml2-2*, *tml1-1 tml2-2*, *tml1-2 tml2-2*, and *sunn-5*. Scale bar = 2 cm. **(B–H)** Magnification of nodules from a representative plant for genotypes **(B)** wild-type R108, **(C)** *tml1-2*, **(D)** *tml1-4*, **(E)** *tml2-1*, **(F)** *tml2-2*, **(G)** *tml1-1 tml2-2*, and **(H)** *tml1-2 tml2-2*. A single root was folded in panel **(H)** to show wider area of nodulation in same picture; **(B–H)**, scale bar = 2 mm.

the xylem poles and did not increase in the nodule. By the time the nodule organized and began to emerge at 72 hpi, this difference in pattern was reinforced, with *MtTML1* highly expressed in the nodule and *MtTML2* expressed in the nodule at the same low level as in tissues of uninoculated plants. Because of the way the laser capture data were collected and displayed, color indicates expression somewhere within the cell types, rather than throughout the area colorized. Examined at the level of single-cell RNA-Seq over a time course of combined experiments harvested at timepoints 0 hpi, 48 hpi, and 96 hpi, the combined transcriptomics data of individual cells responding to rhizobia showed that both *MtTML* genes were expressed in the pericycle cells and vascular bundles, but *MtTML1* was expressed in different cell lineages than *MtTML2* in response to rhizobia (Pereira et al., 2024). Observation of expression levels in undissected root segments over time revealed that both *MtTML* genes were induced twofold to threefold in wild type responding to rhizobia over 72 hours, as well as in the hypernodulation mutant *sunn-4* responding to rhizobia over 72 hours (Schnabel et al., 2023). However, *MtTML1* expression did not begin to decrease over this time frame in the *sunn-4* mutant, while *MtTML2* did. Taken together, the data imply that *MtTML1* and *MtTML2* expression is dynamic and changes between tissues and over time in nodulation; *MtTML1* has higher expression in cortical cells and nodules, whereas *MtTML2* is expressed mainly in the pericycle and vasculature.

tml1 mutants show evidence of transcriptional adaptation

Genetic compensation can occur through several mechanisms, but transcriptional adaptation, in which degradation of the mutant mRNA transcript triggers the increased expression of a paralog or family member (El-Brolosy et al., 2019), is straightforward to test. Using real-time quantitative PCR, we measured the expression of

10.3389/fpls.2024.1504404

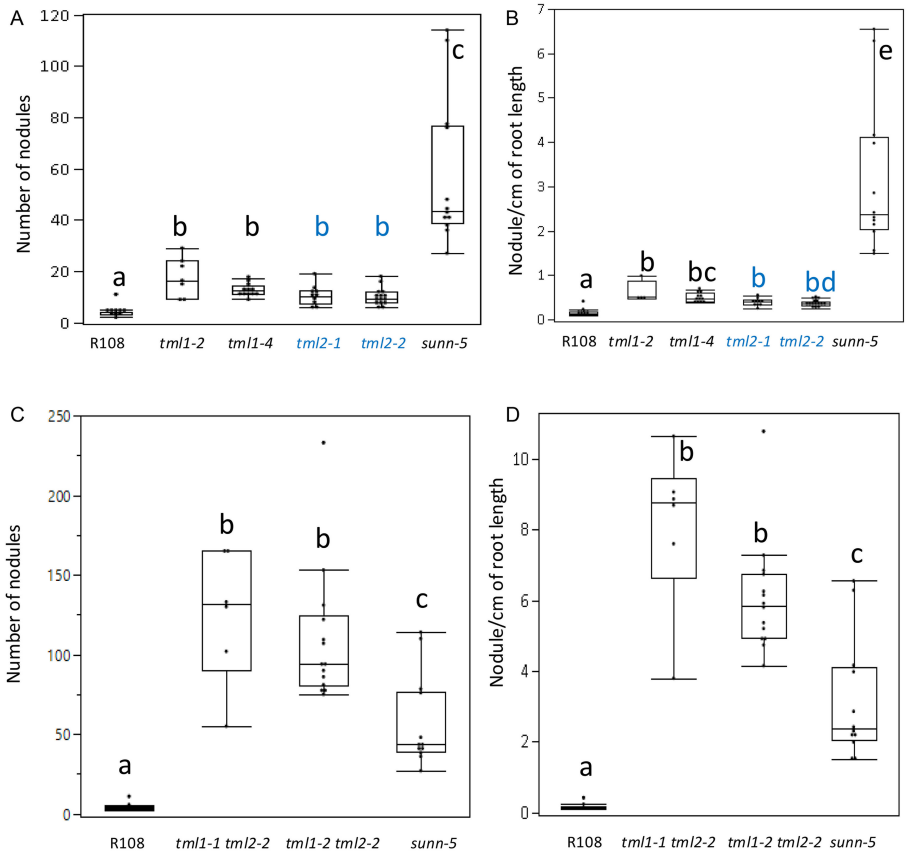

FIGURE 4
Nodulation phenotypes of single and double mutant lines in *MtTML1* and *MtTML2* genes. **(A)** Nodule number and **(B)** nodules per cm root length at 10 dpi of wild type, single mutant single mutant (*tml1* in black and *tml2* in blue), *sunn-5* plants from the same experiment in Figure 3. N = 12 plants for R108 wild type and N = 15 plants for *sunn-5* in all graphs. N = 7 plants for *tml1-2*, N = 10 for *tml1-4*, N = 11 for *tml2-1*, and N = 19 for *tml2-2*. Groups not connected by the same letter are statistically different. **(C)** Nodule number and **(D)** nodules per cm root length at 10 dpi of wild type, double mutant, and *sunn-5* plants from the same experiment in Figure 3. Groups not connected by the same letter are statistically different. N = 8 plants for *tml1-1 tml 2-2* and N = 14 for the *tml1-2 tml2-2* double mutant. Significant differences between means were tested by Tukey's comparison for all pairs or non-parametric Steel–Dwass comparison (see Materials and Methods for detailed description). Dots indicate values for individual plants.

one wild-type *MtTML* gene when the other *MtTML* was mutated. In the roots of wild-type R108 and plants containing either a *tml2* or *tml1* mutant transcript, there was no statistical difference in the expression of the wild-type *MtTML* message in the absence of rhizobia (0 hpi), and all plants showed statistical increases in the expression of the examined transcript from the uninoculated level (0 hpi) compared to 72 h after inoculation with rhizobia (72 hpi) ($p < 0.05$) (Figures 5B, C). In the *tml2* mutant, the expression level of *MtTML1* at 72 hpi was statistically equivalent to that of the wild type at 72 hpi, showing no evidence of genetic compensation (Figure 5B). However, in the *tml1* mutant, the expression level of *MtTML2* is increased compared with that of the wild type at 72 hpi ($p < 0.05$) (Figure 5C), suggesting that the loss of a functional copy of *MtTML1* increases the expression of *MtTML2*, but not vice versa. The change in the level of *MtTML1* expression at 72 hpi versus 0 hpi in wild-type plants (2.5-fold) is half that of *MtTML2* at 72 hpi versus 0 hpi in wild-type plants (fivefold), which could make statistically significant differences in *MtTML1* expression harder to detect using this method.

Phenotypic effects of heterozygosity appear in segregation of double TML mutants

Following the observation that the expression of the wild-type *MtTML2* gene increased in a plant containing a mutation in *MtTML1* but did not fully rescue the nodule number phenotype of the *tml1* mutant, we wondered if there is an effect on the nodulation due to heterozygosity of mutant allele. While an intermediate nodule number for plants heterozygous for a *tml* mutation may be difficult to detect given the small size of the effect on nodule number of a single mutation (twofold to threefold change increase in single mutants; Figure 4A), the magnitude of the phenotype of double mutants could allow a nodule number difference to be detectable when plants are homozygous for one mutant allele and heterozygous for the other.

We examined two populations of progeny obtained from selfing plants homozygous for one *tml* mutation and heterozygous for the other, *tml1-2*/TML1 *tml2-2* and *tml1-2 tml2-2*/TML2. A discrete

10.3389/fpls.2024.1504404

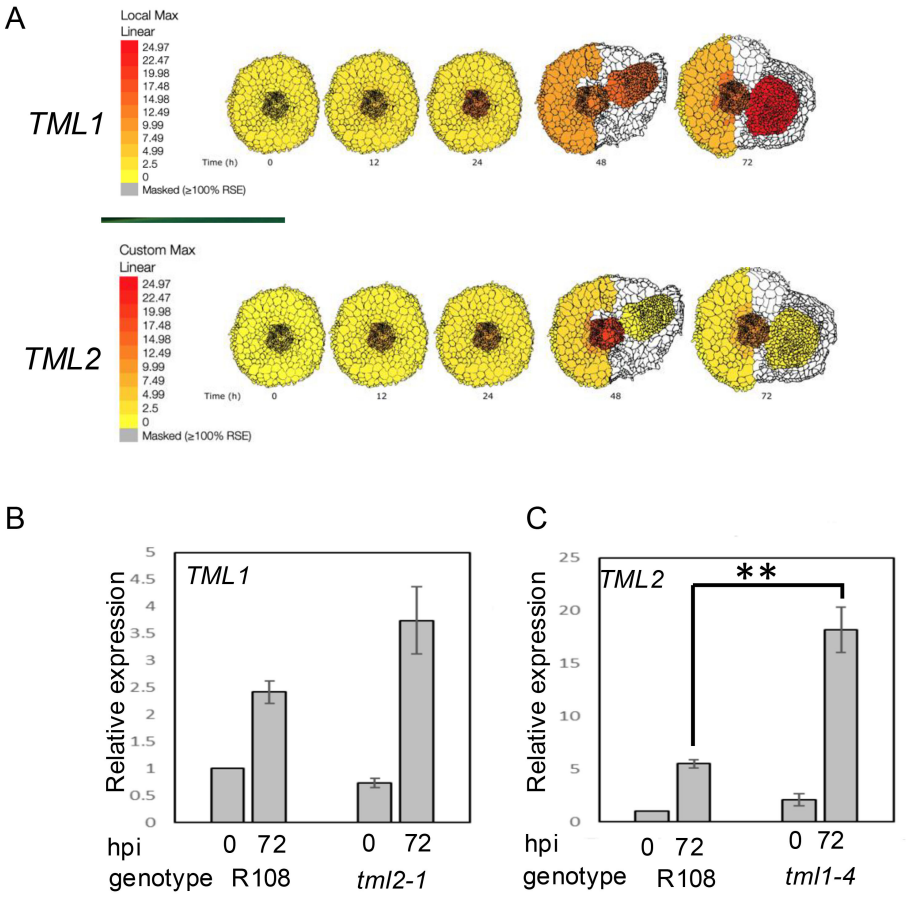

FIGURE 5
Spatiotemporal and differential expression of *MtTML* genes over 72 hours in plants responding to rhizobia. **(A)** Diagrams produced from ePlant resource (Schnabel et al., 2023) with gradient display adjusted to identical color representation to allow comparison of the expression levels as well as localization of *TML1* and *TML2* across time in wild-type roots responding to rhizobia up to 72 hpi. **(B)** Relative expression of *TML1* in a *tml2-2* mutant at 0 and 72 hours post-inoculation (hpi), normalized to wild type at 0 hpi. **(C)** Relative expression of *TML2* in a *tml1-4* mutant at 0 and 72 hours post-inoculation normalized to wild type at 0 hpi. Note Y-axis in B is five times the Y-axis in **(A)**. **p < 0.05. Each graph is the results of three technical replicates of each of three biological replicates from 10 plants compared to the reference gene PIK (Kakar et al., 2008).

recessive phenotype should segregate nodule number phenotypes in a 3:1 Mendelian ratio. While nodule number is a qualitative trait, both populations segregated a broader distribution of nodule number phenotypes with some bi-modal characteristics (Supplementary Figure 2). To test our hypothesis that this distribution of phenotypes is due to changes in the inheritance of the segregating wild-type copy, we used the progeny of plants homozygous for *tml2-2* and segregating *tml1-2*. Out of 141 progenies, a random set of 84 (~60%) of the population was tested by PCR. The PCR-tested progeny were verified for the expected 1:2:1 genotypic segregation using Pearson's chi-square test ($\chi^2 = 7.13$, with 2 degrees of freedom) (Figure 6A). The analysis revealed that plants wild type for the segregating allele had a mean of 22.5 nodules, plants heterozygous for the segregating allele had a mean of 43.8 nodules, and plants homozygous for both mutant alleles had a mean of 100.3 nodules. Each of the three groups was significantly different from each other in Tukey's all-pair comparison ($p < 0.001$) (Figures 6B, C), supporting a phenotypic effect of heterozygosity on the nodule number phenotype.

tml double mutants have minor effects on arbuscular mycorrhizal symbiosis

Many AON mutants also have hyper-mycorrhizal phenotypes, and *miRNA2111* is induced upon phosphate starvation even in *Arabidopsis* (Hsieh et al., 2009), which does not form symbiotic associations with rhizobia or AM fungi. Expecting an increase in AM fungal root colonization, the *tml1-1*, *tml2-2*, and *tml1-2*, *tml2-2* double mutants were tested for a mycorrhizal phenotype with the AM fungus *R. irregularis*. No overall root length colonization difference between double mutants and wild types was observed under our growth conditions at 4.5 weeks post-inoculation (Figure 7A). However, in the same experiment at 6 weeks post-inoculation, a small but statistically significant increase in AM fungal root length colonization was observed for the *tml1-2 tml2-2* double mutant relative to R108 wild-type controls, but not the *tml1-1 2-2* allele (Figure 7A). Arbuscule morphology appeared normal in the mutants (Figures 7B–D). Together, these data suggest that *MtTML1* and *MtTML2* may play a minor role in AM

10.3389/fpls.2024.1504404

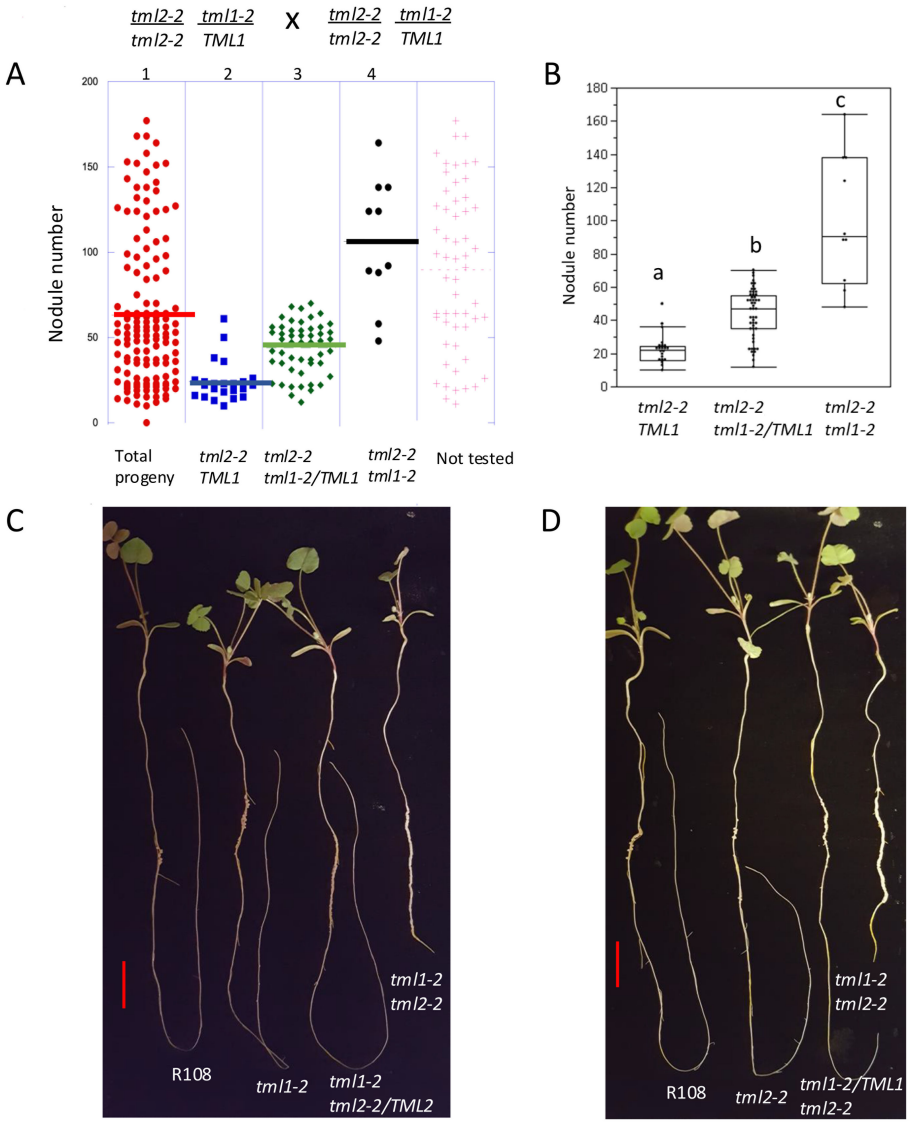

FIGURE 6
Molecular genotype analysis and photographs supporting heterozygous effect. **(A)** Testing 60% (84) of the total population of 141 (indicated in red dots in panel 1) broken down in panels by molecular genotype determined by PCR. Blue dots (panel 2) are homozygous wild type *TML1*, green dots (panel 3) are heterozygous *tml1/TML1*, and black dots (panel 4) are homozygous *tml1/tml1*. Lines indicate median nodule number for each group. **(B)** Box plot showing the distribution of nodule number in each genotype. Groups indicated by different letters are significantly different as tested by Tukey all pair test ($p<0.001$). **(C)** One representative plant per genotype L to R: R108 (wild type), *tml1-2*, *tml1-2 tml2-2/TML2*, *tml1-2 tml2-2* and **(D)** R108 (wild type), *tml2-2*, *tml1-2/TML1 tml2-2*, *and tml1-2 tml2-2*. Scale bar = 2 cm.

symbiosis, although their impact appears to depend on the timepoint measured and the mutant allele.

Discussion

While the *TML* gene was first identified and investigated in *L. japonicus* (Ishikawa et al., 2008; Yokota et al., 2009; Magori et al., 2009), legumes and most dicots examined contain two copies of a *TML*-like gene, with tomato and *L. japonicus* as outliers (Takahara et al., 2013). Based on our ability to only identify one *TML* copy in the monocots we analyzed, we suspect an ancestral gene duplication early in the legume lineage, followed by the loss of a copy in *L. japonicus*. Dicots containing more than one copy appear to be the result of genome duplications and are more closely related in sequence to each other than to either legume *TML*, hence the a, b labeling in Figure 1. As is common for many genes in soybean, the *Glycine max* genome contains two copies of *TML1*. Since monocots and dicots diverged approximately 200 million years ago (Wolfe et al., 1989), and legumes even later, enough time has passed for the genes to have adopted divergent functions, but this work suggests that any divergence within legumes is complex, and the genes have evolved to give synergistic effects in some of the symbiotic phenotypes tested and none in others.

Given the moderate effect of RNAi on the *M. truncatula TML*s on nodulation phenotypes (Gautrat et al., 2019), we expected the

10.3389/fpls.2024.1504404

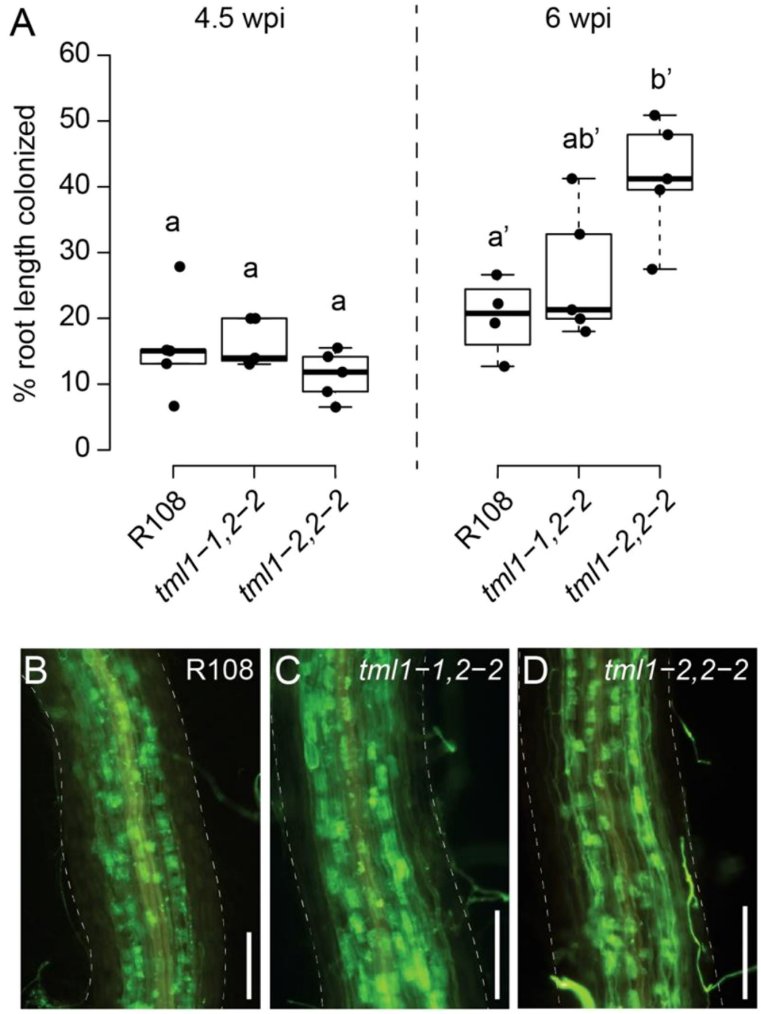

FIGURE 7
Arbuscular mycorrhiza phenotype of *tml1*, *tml2* double mutants. **(A)** Overall root length colonization in R108, *tml1-1*, *tml2-2*, and *tml1-1*, *tml2-2* is similar at 4.5 weeks post-inoculation (wpi), whereas at 6 wpi, increased colonization levels were observed in the *tml1-2*, *tml2-2* double mutants relative to R108 controls. Statistical differences were calculated separately for each timepoint (ANOVA followed by Tukey's HSD; different letters denote significant differences in pairwise comparisons with $p<0.05$). **(B)** Representative image of *Rhizophagus irregularis* symbiotic structures in an R108 wild-type root (6wpi). **(C)** Representative image of a *R. irregularis*-colonized root of a *tml1-1 tml 2-2* double mutant (6wpi). **(D)** Representative image of a *R. irregularis-colonized* root of a *tml1-2 tml2-2* double mutant (6 wpi). **(B–D)** *R. irregularis* fungal structures are visualized with WGA-Alexafluor488. *M. truncatula* root is outlined with a dashed line. Scale bar: 250 µm.

strong genetic mutants created in this study (stop codons early in the gene) to have a larger effect on phenotype than observed in Gautrat et al. (2019). However, all single mutations, predicted to result in highly truncated proteins if translated, displayed only a twofold to threefold increase in the number of nodules compared to wild-type plants (Figure 4). In sharp contrast, a mutation in the single copy of *TML* in *L. japonicus* results in eight times more nodules than the wild type (Magori et al., 2009). When both copies of *TML* were disrupted in *M. truncatula*, the nodule number phenotype was logarithmically increased, exceeding that observed for *sunn* mutants (Figure 4) and the *L. japonicus tml* mutant (Magori et al., 2009). In our aeroponic system (Cai et al., 2023), all plants encountered rhizobia at the same time, leading to a distinct zone of nodulation even in AON mutants such as *sunn* and *rdn1* (Schnabel et al., 2005, 2011). Interestingly, while we observed the same effect in single *tml* mutants, the double mutants nodulated along the entire root (Figure 3), suggesting that competence to nodulate may be more than just an on/off switch (Laffont and Frugier, 2024) and that other characteristics such as the extent of the nodulation zone or the speed of nodule development could be regulated by a signal dependent on both TML proteins.

The observation of transcriptional adaptation in *tml1* mutants (increased expression of the *MtTML2* gene during nodulation) (Figure 5C) could suggest some overlap in function between the two genes. *MtTML1* is expressed in the nodules at 72 hpi (likely the nodule vasculature) based on Pereira et al. (2024), and *MtTML2* is not (Figure 5A). Nevertheless, the loss of *MtTML1* results in the increased expression of *MtTML2*, which is normally not expressed in the nodules (Figure 5C). The identification of a slightly increased

nodule number phenotype in *tml* single mutants (Figure 4) and a distinct nodule number phenotype in *TML* heterozygotes (Figure 6) also suggests that the two genes are not completely redundant. As noted in the description of the results for Figure 5, because the fold change observed in *MtTML1* expression between 0 hpi and 72 hpi is much smaller than that of *MtTML2*, genetic compensation for *MtTML1* in *tml2* mutants could exist but is too small for observation of a statistically significant change in expression in our experimental design. Even if genetic compensation does not occur, an overlap of function could explain the small effect on nodule number in single mutants. The differences in mean nodule number for *tml1-2 TML1* heterozygotes segregating in a *tml2-2* background versus plants carrying a wild-type allele in the same background combined with the additional observation of a similar distribution of nodule number in *tml2-2 TML2* heterozygotes segregating in a *tml1-2* background suggest that the combined level of wild-type *MtTML* message (*MtTML1* + *MtTML2*) may affect the number of nodules formed.

Additional causes for synergistic gene interaction (Pérez-Pérez et al., 2009) could apply to the synergy observed in *MtTML* mutants. The single and double mutant alleles in this analysis contain premature stop codons predicted to result in a truncated protein without any functional domains (Figure 2). The prediction of complete loss of function (null) mutations in *MtTML* rules out the possibility that the synergistic phenotype is the result of hypomorphic alleles, but synergy can also be observed when the products of two genes interact in a multimeric protein complex; mutation of one component leads to fewer monomers, resulting in fewer functional protein complex in a dose-dependent manner. While purely speculative, one possible explanation for both the individual phenotypes and the synergy observed is that the two proteins form homo- or heterodimers as part of their downstream signaling. It is also possible the two proteins may function together bound to a third target, such as a promoter or a transcription factor, or provide the localization signal to bring a factor into the nucleus.

Given that TML regulation of AON is predicted to result from the destruction of the mRNA by miR2111, we suggest that the synergy comes from a dosage dependence of the wild-type message combined with genetic compensation. The lower transcript levels of both *MtTML1* and *MtTML2* in roots under low N conditions are correlated with root competence to nodulation (0 hpi in Figure 5), whereas higher transcript levels of both genes are correlated with inhibition of nodulation after rhizobial inoculation later in time (Gautrat et al., 2020).

The current AON model is highly simplified, involving signal transduction in both space and time based on evidence gathered by multiple groups in multiple systems and species. We do not know the half-life of the MtTML proteins, which would affect the length of time between detecting decreased mRNA and the action of the MtTML proteins in halting nodulation; split root analysis suggests the AON systemic signal has an effect on nodule number within 72 hpi in *M. truncatula* (Kassaw et al., 2015), but no decreased *TML* expression was detected during this time in our system. What appear to be differences in *MtTML* expression results between our work and others can explained by differences in timing and setup between experiments—the decreased *MtTML* expression data (Gautrat et al., 2020) were collected at 5 dpi in whole roots on plates versus the increase of *MtTML1* in Schnabel et al. (2023) at 3 dpi in nodulating segments of roots in an aeroponic chamber. Our results in general support the position of TML in the AON model but also provide evidence that the functions of the individual *MtTML* genes are not completely redundant.

With regard to the role of *MtTML*s in AOM, AON and AOM share multiple common components including common LRR-RLKs that perceive distinct CLE peptides specific to nodulation and AM symbiosis, respectively (Roy and Müller, 2022). When legumes are inoculated with rhizobia and AM fungi, the two symbioses influence each other (Catford et al., 2003), potentially by competing for carbon. However, we previously reported that the AON regulator MtCLE13 does not influence AM symbiosis, suggesting that AON and AOM have symbiosis-specific signaling outcomes (Müller et al., 2019). Because the distinct CLE signals mediating AON, AOM, and P and N regulation of nodulation and AM symbiosis converge at the same LRR-RLK SUNN but result in at least partially distinct outcomes, it appears that plants can distinguish between the signals. Along these lines, the *M. truncatula* pseudokinase *MtCORYNE* was found to be involved in mediating AON signaling downstream of *MtCLE12* and *MtCLE13* (Nowak et al., 2019), whereas it is partially dispensable for AOM signaling by *MtCLE53* (Orosz et al., 2024). Similarly, while our results demonstrate that *M. truncatula TML1* and *TML2* are important components of AON signaling, they seem to play a weaker role in AOM. We only observed small increases in AM fungal root colonization in the *tml1-2*, *2-2* double mutant (in which *MtTML1* is disrupted by a 111-bp deletion) and no detectable increase when using the *tml1-1*, *2-2* allele, which is caused by a nonsense mutation near the N-terminus of the protein (Figures 2, 7), in which case occasional stop codon read-through may produce a truncated but at least partially functional MtTML1 protein (Zhang et al., 2024). Such phenotypic difference between the two alleles was not observed in our nodulation experiments (Figure 4), presumably because the nodulation phenotype is much stronger than the relatively mild AM symbiosis phenotype. In addition, P and N regulate nodulation and AM symbiosis through similar pathways converging at the same LRR-RLK SUNN (Roy and Müller, 2022). Although we found only a weak phenotype in one of the double mutant alleles tested, our results suggest *MtTML* genes play at least a small role in AM symbiosis regulation. One tempting hypothesis is that the effect of TML on AM symbiosis stems through intersection with nutrient homeostasis signaling. miR2111, which targets *TML*, is also regulated by N- and P-starvation-induced CEP peptides that signal through the RLK CRA2 to regulate nodulation and AM symbiosis, respectively (Laffont et al., 2019, 2020; Ivanovici, 2021; Ivanovici et al., 2023; Lepetit and Brouquisse, 2023).

This study uncovered the non-redundant but synergistic role of MtTML1 and MtTML2 in AON and AOM and opens a new avenue for definitive additional experiments in *M. truncatula* to refine and fill in gaps in the model with the *MtTML* mutants we have created. It is unknown how *SUNN* signaling results in changes in miR2111 expression in the shoot or whether the destruction of *TML* RNA by miR2111 binding in the root affects further *TML* expression. It is

unknown how the TML proteins exert their effects and through what other proteins (although the presence of nuclear localization signals may suggest interaction with transcription factors). It is possible that there are regulatory steps that involve loading and unloading in the vasculature or import to the nucleus that involves other proteins that TML reacts with. The mutants described here will allow these and other important questions to be investigated.

Data availability statement

The datasets presented in this study can be found in online repositories. The names of the repository/repositories and accession number(s) can be found in the article/Supplementary Material.

Author contributions

DC: Formal analysis, Investigation, Methodology, Validation, Visualization, Writing – original draft, Writing – review & editing. ES: Formal analysis, Investigation, Methodology, Writing – review & editing. MK: Formal analysis, Investigation, Validation, Writing – review & editing. EL: Formal analysis, Investigation, Visualization, Writing – review & editing. LM: Formal analysis, Funding acquisition, Investigation, Methodology, Supervision, Visualization, Writing – original draft, Writing – review & editing. JF: Conceptualization, Formal analysis, Funding acquisition, Investigation, Methodology, Supervision, Visualization, Writing – original draft, Writing – review & editing.

Funding

The author(s) declare financial support was received for the research, authorship, and/or publication of this article. This work was supported by The National Science Foundation of the United States (NSF 1733470) to JF to characterize nodulation mutants and support Diptee Chaulagain, and United States Department of Agriculture-NIFA (USDA-NIFA 2022-67013-36881) to LM to support study of AM symbiosis regulation.

Acknowledgments

We acknowledge Clemson Light Imaging Facility and Dr. Terri Bruce, Rhonda Powell, and J. Conrad Epps for training and assistance with the Leica THUNDER Imager equipment use. We acknowledge Hemani Patel, an undergraduate mentored by Diptee Chaulagain, for the PCR work on segregating single mutants. We thank Dr. Li Wen for teaching *M. truncatula* crossing to DC and Dr. Yuanling Chen for tissue culture tips and troubleshooting.

Conflict of interest

The authors declare that the research was conducted in the absence of any commercial or financial relationships that could be construed as a potential conflict of interest.

Generative AI statement

The author(s) declare that no Generative AI was used in the creation of this manuscript.

Publisher's note

Supplementary material

The Supplementary Material for this article can be found online at: https://www.frontiersin.org/articles/10.3389/fpls.2024.1504404/full#supplementary-material

SUPPLEMENTARY FIGURE 1
Multiplexed targeted CRISPR/Cas9 mutagenesis in *TML* genes using Csy4 plasmid. **(A)** Schematic diagram of polycistronic gene construct used in pDIRECT_23C+TML1/2 for making tml1/tml2 double mutants and **(B)** in pDIRECT_23C+TML1 for making tml1 mutant **(C)** Maps of *MtTML1* and *MtTML2* genes showing the location of targets. PAM for each target is underlined. Blue boxes indicate CDS, grey boxes indicate UTR, red rectangles indicate predicted miRNA2111 binding sites, and lines indicate introns; arrow at the right end of grey box points to 3′ end of gene. **(D)** CRISPR effects on DNA resulting in *tml1* alleles, displayed in relation to the target sequences (yellow) and PAM sequences (green). Base changes and deletions are in red. The *tml1-4* allele has a 107 bp deletion that removes 48bp upstream of the transcription start site and 59bp in the CDS, including target 1. **(E)** CRISPR effects on DNA in the *tml2* allele, displayed in relation to the target sequences (yellow) and PAM sequences (green). Base changes and deletions are in red.

SUPPLEMENTARY FIGURE 2
Distribution of nodulation number phenotypes suggests heterozygous effect. Distribution plots of two populations of progeny from selfing of plant on X axis. Red dots are individual plant nodule numbers from *tml2-2* mutant plants segregating one wild type *TML1* allele, blue squares are *tml1-2* mutants segregating one wild type *TML2* allele.

SUPPLEMENTARY TABLE 1
Genes used in Maximum Likelihood tree in Figure 1.

SUPPLEMENTARY TABLE 2
Primers used in this manuscript.

References

Bashyal, S., Gautam, C. K., and Müller, L. M. (2024). CLAVATA signaling in plant–environment interactions. *Plant Physiol.* 194, 1336–1357. doi: 10.1093/plphys/kiad591

Cai, J., Veerappan, V., Arildsen, K., Sullivan, C., Piechowicz, M., Frugoli, J., et al. (2023). A modified aeroponic system for growing plants to study root systems. *Plant Methods*. doi: 10.1186/s13007-023-01000-6

Catford, J.-G., Staehelin, C., Lerat, S., Piché, Y., and Vierheilig, H. (2003). Suppression of arbuscular mycorrhizal colonization and nodulation in split-root systems of alfalfa after pre-innoculation and treatment with Nod factors. *J. Exp. Bot.* 54, 1481–1487. doi: 10.1093/jxb/erg156

Čermák, T., Curtin, S. J., Gil-Humanes, J., Čegan, R., Kono, T. J., Konečná, E., et al. (2017). A multipurpose toolkit to enable advanced genome engineering in plants. *Plant Cell* 29, 1196–1217. doi: 10.1105/tpc.16.00922

Chaulagain, D., and Frugoli, J. (2021). The regulation of nodule number in legumes is a balance of three signal transduction pathways. *Int. J. Mol. Sci*. doi: 10.3390/ijms22031117

Chaulagain, D., Schnabel, E., Crook, A., Bashyal, S., Müller, L., and Frugoli, J. (2023). A mutation in mediator subunit MED16A suppresses nodulation and increases arbuscule density in medicago truncatula. *J. Plant Growth Regul.*, 1–19. doi: 10.1007/s00344-023-10993-2

Crook, A. D., Schnabel, E. L., and Frugoli, J. A. (2016). The systemic nodule number regulation kinase SUNN in Medicago truncatula interacts with MtCLV2 and MtCRN. *Plant J.* 88, 108–119. doi: 10.1111/tpj.2016.88.issue-1

Dai, X., Hu, Q., Cai, Q., Feng, K., Ye, N., Tuskan, G. A., et al. (2014). The willow genome and divergent evolution from poplar after the common genome duplication. *Cell Res.* 24, 1274–1277. doi: 10.1038/cr.2014.83

El-Brolosy, M. A., Kontarakis, Z., Rossi, A., Kuenne, C., Günther, S., Fukuda, N., et al. (2019). Genetic compensation triggered by mutant mRNA degradation. *Nature* 568, 193–197. doi: 10.1038/s41586-019-1064-z

Engler, C., Gruetzner, R., Kandzia, R., and Marillonnet, S. (2009). Golden gate shuffling: a one-pot DNA shuffling method based on type IIs restriction enzymes. *PloS One* 4, e5553. doi: 10.1371/journal.pone.0005553

Engler, C., Kandzia, R., and Marillonnet, S. (2008). A one pot, one step, precision cloning method with high throughput capability. *PloS One* 3, e3647. doi: 10.1371/journal.pone.0003647

Ferguson, B. J., Mens, C., Hastwell, A. H., Zhang, M., Su, H., Jones, C. H., et al. (2019). Legume nodulation: the host controls the party. *Plant Cell Environ.* 42, 41–51. doi: 10.1111/pce.13348

Gao, X., and Guo, Y. (2012). CLE peptides in plants: proteolytic processing, structure-activity relationship, and ligand-receptor interactions. *J. Integr. Plant Biol.* 54, 738–745. doi: 10.1111/j.1744-7909.2012.01154.x

Gautrat, P., Laffont, C., and Frugier, F. (2020). Compact Root Architecture 2 Promotes Root Competence for Nodulation through the miR2111 Systemic Effector. *Curr. Biol.* 30, 1339–1345.e1333. doi: 10.1016/j.cub.2020.01.084

Gautrat, P., Laffont, C., Frugier, F., and Ruffel, S. (2021). Nitrogen systemic signaling: from symbiotic nodulation to root acquisition. *Trends Plant Sci.* 26, 392–406. doi: 10.1016/j.tplants.2020.11.009

Gautrat, P., Mortier, V., Laffont, C., De Keyser, A., Fromentin, J., Frugier, F., et al. (2019). Unraveling new molecular players involved in the autoregulation of nodulation in Medicago truncatula. *J. Exp. Bot.* 70, 1407–1417. doi: 10.1093/jxb/ery465

Genre, A., Lanfranco, L., Perotto, S., and Bonfante, P. (2020). Unique and common traits in mycorrhizal symbioses. *Nat. Rev. Microbiol.* 18, 649–660. doi: 10.1038/s41579-020-0402-3

Giovannetti, M., and Mosse, B. (1980). AN EVALUATION OF TECHNIQUES FOR MEASURING VESICULAR ARBUSCULAR MYCORRHIZAL INFECTION IN ROOTS. *New Phytol.* 84, 489–500. doi: 10.1111/j.1469-8137.1980.tb04556.x

Hood, E. E., Gelvin, S. B., Melchers, L. S., and Hoekema, A. (1993). New agrobacterium helper plasmids for gene-transfer to plants. *Transgenic Res.* 2, 208–218. doi: 10.1007/BF01977351

Hsieh, L.-C., Lin, S.-I., Shih, A. C.-C., Chen, J.-W., Lin, W.-Y., Tseng, C.-Y., et al. (2009). Uncovering small RNA-mediated responses to phosphate deficiency in Arabidopsis by deep sequencing. *Plant Physiol.* 151, 2120–2132. doi: 10.1104/pp.109.147280

Ivanovici, A. S. L. (2021). *Signals and perCEPtion: diverse roles for C-Terminally Encoded Peptides in symbiosis, root system gravitropism, and pathogen response in Medicago truncatula and Arabidopsis thaliana* (Australia: The Australian National University).

Ivanovici, A., Laffont, C., Larrainzar, E., Patel, N., Winning, C. S., Lee, H.-C., et al. (2023). The Medicago SymCEP7 hormone increases nodule number via shoots without compromising lateral root number. *Plant Physiol.* 191, 2012–2026. doi: 10.1093/plphys/kiad012

Kakar, K., Wandrey, M., Czechowski, T., Gaertner, T., Scheible, W.-R., Stitt, M., et al. (2008). A community resource for high-throughput quantitative RT-PCR analysis of transcription factor gene expression in Medicago truncatula. *Plant Methods* 4, 18. doi: 10.1186/1746-4811-4-18

Karlo, M., Boschiero, C., Landerslev, K. G., Blanco, G. S., Wen, J., Mysore, K. S., et al. (2020). The CLE53–SUNN genetic pathway negatively regulates arbuscular mycorrhiza root colonization in Medicago truncatula. *J. Exp. Bot.* 71, 4972–4984. doi: 10.1093/jxb/eraa193

Kassaw, T., Bridges, W., and Frugoli, J. (2015). Multiple autoregulation of nodulation (AON) signals identified through split root analysis of M. truncatula sunn and rdn1 mutants. *Plants* 4, 209–224. doi: 10.3390/plants4020209

Kassaw, T., Nowak, S., Schnabel, E., and Frugoli, J. (2017). ROOT DETERMINED NODULATION1 Is Required for M. truncatula CLE12, But Not CLE13, Peptide Signaling through the SUNN Receptor Kinase. *Plant Physiol.* 174, 2445–2456. doi: 10.1104/pp.17.00278

Laffont, C., and Frugier, F. (2024). Rhizobium symbiotic efficiency meets CEP signaling peptides. *New Phytol.* 24, 24–27. doi: 10.1111/nph.19367

Laffont, C., Huault, E., Gautrat, P., Endre, G., Kalo, P., Bourion, V., et al. (2019). Independent regulation of symbiotic nodulation by the SUNN negative and CRA2 positive systemic pathways. *Plant Physiol.* 180, 559–570. doi: 10.1104/pp.18.01588

Laffont, C., Ivanovici, A., Gautrat, P., Brault, M., Djordjevic, M. A., and Frugier, F. (2020). The NIN transcription factor coordinates CEP and CLE signaling peptides that regulate nodulation antagonistically. *Nat. Commun.* 11. doi: 10.1038/s41467-020-16968-1

Lepetit, M., and Brouquisse, R. (2023). Control of the rhizobium–legume symbiosis by the plant nitrogen demand is tightly integrated at the whole plant level and requires inter-organ systemic signaling. *Front. Plant Sci.* 14. doi: 10.3389/fpls.2023.1114840

Ma, X., and Liu, Y. G. (2016). CRISPR/Cas9-based multiplex genome editing in monocot and dicot plants. *Curr. Protoc. Mol. Biol.* 115. doi: 10.1002/0471142727.2016.115.issue-1

Magori, S., Oka-Kira, E., Shibata, S., Umehara, Y., Kouchi, H., Hase, Y., et al. (2009). TOO MUCH LOVE, a root regulator associated with the long-distance control of nodulation in Lotus japonicus. *Mol. Plant-Microbe Interact.* 22, 259–268. doi: 10.1094/MPMI-22-3-0259

Meixner, C., Ludwig-Müller, J., Miersch, O., Gresshoff, P., Staehelin, C., and Vierheilig, H. (2005). Lack of mycorrhizal autoregulation and phytohormonal changes in the supernodulating soybean mutant nts1007. *Planta* 222, 709–715. doi: 10.1007/s00425-005-0003-4

Morandi, D., Sagan, M., Prado-Vivant, E., and Duc, G. (2000). Influence of genes determining supernodulation on root colonization by the mycorrhizal fungus Glomus mosseae in Pisum sativum and Medicago truncatula mutants. *Mycorrhiza* 10, 37–42. doi: 10.1007/s005720050285

Mortier, V., Den Herder, G., Whitford, R., Van de Velde, W., Rombauts, S., D'Haeseleer, K., et al. (2010). CLE peptides control Medicago truncatula nodulation locally and systemically. *Plant Physiol.* 153, 222–237. doi: 10.1104/pp.110.153718

Mortier, V., De Wever, E., Vuylsteke, M., Holsters, M., and Goormachtig, S. (2012). Nodule numbers are governed by interaction between CLE peptides and cytokinin signaling. *Plant J.* 70, 367–376. doi: 10.1111/j.1365-313X.2011.04881.x

Müller, L. M., Flokova, K., Schnabel, E., Sun, X., Fei, Z., Frugoli, J., et al. (2019). A CLE–SUNN module regulates strigolactone content and fungal colonization in arbuscular mycorrhiza. *Nat. Plants* 5, 933–939. doi: 10.1038/s41477-019-0501-1

Nowak, S., Schnabel, E., and Frugoli, J. (2019). The Medicago truncatula CLAVATA3-LIKE CLE12/13 signaling peptides regulate nodule number depending on the CORYNE but not the COMPACT ROOT ARCHITECTURE2 receptor. *Plant Signaling Behav.* 14, 1598730. doi: 10.1080/15592324.2019.1598730

Okuma, N., and Kawaguchi, M. (2021). Systemic optimization of legume nodulation: A shoot-derived regulator, miR2111. *Front. Plant Sci.* 12, 682486. doi: 10.3389/fpls.2021.682486

Okuma, N., Soyano, T., Suzaki, T., and Kawaguchi, M. (2020). MIR2111-5 locus and shoot-accumulated mature miR2111 systemically enhance nodulation depending on HAR1 in Lotus japonicus. *Nat. Commun.* 11, 5192. doi: 10.1038/s41467-020-19037-9

Oldroyd, G. E., and Leyser, O. (2020). A plant's diet, surviving in a variable nutrient environment. *Science* 368, eaba0196. doi: 10.1126/science.aba0196

Orosz, J., Lin, E. X., Lindsay, P., Kappes, M., Bashyal, S., Everett, H., et al. (2024). *Medicago truncatula CORYNE* regulates inflorescence meristem branching, nutrient signaling, and arbuscular mycorrhizal symbiosis. *bioRxiv*, 2024–09.

Pant, B. D., Musialak-Lange, M., Nuc, P., May, P., Buhtz, A., Kehr, J., et al. (2009). Identification of nutrient-responsive Arabidopsis and rapeseed microRNAs by comprehensive real-time polymerase chain reaction profiling and small RNA sequencing. *Plant Physiol.* 150, 1541–1555. doi: 10.1104/pp.109.139139

Pereira, W. J., Boyd, J., Conde, D., Triozzi, P. M., Balmant, K. M., Dervinis, C., et al. (2024). The single-cell transcriptome program of nodule development cellular lineages in medicago truncatula. *Cell Rep*. doi: 10.1016/j.celrep.2024.113747

Pérez-Pérez, J. M., Candela, H., and Micol, J. L. (2009). Understanding synergy in genetic interactions. *Trends Genet.* 25, 368–376. doi: 10.1016/j.tig.2009.06.004

Putnoky, P., Petrovics, G., Kereszt, A., Grosskopf, E., Ha, D., Banfalvi, Z., et al. (1990). Rhizobium meliloti lipopolysaccharide and exopolysaccharide can have the same function in the plant-bacterium interaction. *J. bacteriology* 172, 5450–5458. doi: 10.1128/jb.172.9.5450-5458.1990

Renny-Byfield, S., Chester, M., Kovařík, A., Le Comber, S. C., Grandbastien, M.-A., Deloger, M., et al. (2011). Next Generation Sequencing Reveals Genome Downsizing in Allotetraploid Nicotiana tabacum, Predominantly through the Elimination of Paternally Derived Repetitive DNAs. *Mol. Biol. Evol.* 28, 2843–2854. doi: 10.1093/molbev/msr112

Roy, S., Liu, W., Nandety, R. S., Crook, A., Mysore, K. S., Pislariu, C. I., et al. (2020). Celebrating 20 years of genetic discoveries in legume nodulation and symbiotic nitrogen fixation. *Plant Cell* 32, 15–41. doi: 10.1105/tpc.19.00279

Roy, S., and Müller, L. M. (2022). A rulebook for peptide control of legume–microbe endosymbioses. *Trends Plant Sci.* doi: 10.1016/j.tplants.2022.02.002

Schnabel, E. L., Chavan, S. A., Gao, Y., Poehlman, W. L., Feltus, F. A., and Frugoli, J. A. (2023). A Medicago truncatula Autoregulation of Nodulation Mutant Transcriptome Analysis Reveals Disruption of the SUNN Pathway Causes Constitutive Expression Changes in Some Genes, but Overall Response to Rhizobia Resembles Wild-Type, Including Induction of TML1 and TML2. *Curr. Issues Mol. Biol.* 45, 4612–4631. doi: 10.3390/cimb45060293

Schnabel, E., Journet, E. P., Carvalho-Niebel, F., Duc, G., and Frugoli, J. (2005). The Medicago truncatula SUNN gene encoding a CLV1-like leucine-rich repeat receptor kinase regulates both nodule number and root length. *Plant Mol. Biol.* 58, 809–822. doi: 10.1007/s11103-005-8102-y

Schnabel, E., Kassaw, T., Smith, L., Marsh, J., Oldroyd, G., Long, S., et al. (2011). The ROOT DETERMINED NODULATION 1 gene regulates nodule number in roots of Medicago truncatula and defines a highly conserved, uncharacterized plant gene family. *Plant Physiol.* 157, 328–340. doi: 10.1104/pp.111.178756

Schnabel, E., Mukherjee, A., Smith, L., Kassaw, T., Long, S., and Frugoli, J. (2010). The lss supernodulation mutant of Medicago truncatula reduces expression of the SUNN gene. *Plant Physiol.* 154, 1390–1402. doi: 10.1104/pp.110.164889

Shultz, J. L., Kurunam, D., Shopinski, K., Iqbal, M. J., Kazi, S., Zobrist, K., et al. (2006). The Soybean Genome Database (SoyGD): a browser for display of duplicated, polyploid, regions and sequence tagged sites on the integrated physical and genetic maps of Glycine max. *Nucleic Acids Res.* 34, D758–D765. doi: 10.1093/nar/gkj050

Sparling, G. P., and Tinker, P. B. (1978). Mycorrhizal infection in pennine grassland. I. Levels of infection in the field. *J. Appl. Ecol.* 15, 943–950. doi: 10.2307/2402789

Tadege, M., Wen, J. Q., He, J., Tu, H. D., Kwak, Y., Eschstruth, A., et al. (2008). Large-scale insertional mutagenesis using the Tnt1 retrotransposon in the model legume Medicago truncatula. *Plant J.* 54, 335–347. doi: 10.1111/j.1365-313X.2008.03418.x

Takahara, M., Magori, S., Soyano, T., Okamoto, S., Yoshida, C., Yano, K., et al. (2013). Too much love, a novel Kelch repeat-containing F-box protein, functions in the long-distance regulation of the legume-Rhizobium symbiosis. *Plant Cell Physiol.* 54, 433–447. doi: 10.1093/pcp/pct022

Tamura, K., Stecher, G., and Kumar, S. (2021). MEGA11: molecular evolutionary genetics analysis version 11. *Mol. Biol. Evol.* 38, 3022–3027. doi: 10.1093/molbev/msab120

Tang, H., Krishnakumar, V., Bidwell, S., Rosen, B., Chan, A., Zhou, S., et al. (2014). An improved genome release (version Mt4. 0) for the model legume Medicago truncatula. *BMC Genomics* 15, 1–14. doi: 10.1186/1471-2164-15-312

Tsikou, D., Yan, Z., Holt, D. B., Abel, N. B., Reid, D. E., Madsen, L. H., et al. (2018). Systemic control of legume susceptibility to rhizobial infection by a mobile microRNA. *Science* 362, 233–236. doi: 10.1126/science.aat6907

Wang, C., Reid, J. B., and Foo, E. (2018). The art of self-control – autoregulation of plant–microbe symbioses. *Front. Plant Sci.* 9, 988. doi: 10.3389/fpls.2018.00988

Wang, C., Velandia, K., Kwon, C.-T., Wulf, K. E., Nichols, D. S., Reid, J. B., et al. (2021). The role of CLAVATA signalling in the negative regulation of mycorrhizal colonization and nitrogen response of tomato. *J. Exp. Bot.* 72, 1702–1713. doi: 10.1093/jxb/eraa539

Wen, L., Chen, Y., Schnabel, E., Crook, A. D., and Frugoli, J. (2019). Comparison of efficiency and time to regeneration of Agrobacterium-mediated transformation methods in Medicago truncatula. *Plant Methods* 15. doi: 10.1186/s13007-019-0404-1

Wolfe, K. H., Gouy, M., Yang, Y.-W., Sharp, P. M., and Li, W.-H. (1989). Date of the monocot-dicot divergence estimated from chloroplast DNA sequence data. *Proc. Natl. Acad. Sci.* 86, 6201–6205. doi: 10.1073/pnas.86.16.6201

Wulf, K., Sun, J., Wang, C., Ho-Plagaro, T., Kwon, C.-T., Velandia, K., et al. (2024). The role of CLE peptides in the suppression of mycorrhizal colonization of tomato. *Plant Cell Physiol.* 65, 107–119. doi: 10.1093/pcp/pcad124

Zakaria Solaiman, M., Senoo, K., Kawaguchi, M., Imaizumi-Anraku, H., Akao, S., Tanaka, A., et al. (2000). Characterization of mycorrhizas formed by Glomus sp. on roots of hypernodulating mutants of Lotus japonicus. *J. Plant Res.* 113, 443–448. doi: 10.1007/PL00013953

Zhang, Y., Li, H., Shen, Y., Wang, S., Tian, L., Yin, H., et al. (2024). Readthrough events in plants reveal plasticity of stop codons. *Cell Rep.* 43. doi: 10.1016/j.celrep.2024.113723